Journal of the Serbian Chemical Society
JSCS-info@shd.org.rs • www.shd.org.rs/JSCS

J. Serb. Chem. Soc. 90 (11) 1383–1399 (2025)
JSCS–5460

Original scientific paper
Published 13 November 2025

Investigation of corrosion causes and failures in the interior metal components of an automobile

JOVANKA N. PEJIĆ[1], BORE V. JEGDIĆ[1], BOJANA M. RADOJKOVIĆ[1]*, ANDJELA R. SIMOVIĆ[1], DUNJA D. MARUNKIĆ[1], BRANIMIR Z. JUGOVIĆ[2] and ALEKSANDRA S. POPOVIĆ[3]

[1]*University of Belgrade, Institute for Chemistry, Technology and Metallurgy, Njegoševa 12, Belgrade,* [2]*Institute of Technical Sciences SASA, Knez Mihailova 35, Belgrade and* [3]*University of Belgrade, Faculty for Technology and Metallurgy, Karnegieva 4, Belgrade, Serbia*

(Received 27 March, revised 17 April, accepted 10 July 2025)

Abstract: The extent of corrosion and the underlying causes of damage to the interior metal components of a one-year-old automobile from a known brand, owned by a rental car company in Serbia, were investigated. The vehicle's interior, including upholstery and carpeting, showed no chemical spills or other damage. The solution obtained after rinsing a carpet sample from the car floor exhibited neutral pH. The corrosion behavior of the analyzed samples was determined using electrochemical impedance spectroscopy (EIS), linear polarization resistance (*LPR*) and linear sweep voltammetry (LSV, Tafel method). X-ray diffraction (XRD) and Fourier-transform infrared spectroscopy (FTIR) analyses showed that corrosion products taken from corroded steel parts contain akaganeite *β*-FeO(OH) and iron (II) chloride. FTIR analysis of the organic coating revealed that the applied epoxy layer was insufficiently crosslinked, making it permeable to moisture and chloride ions. Electrochemical corrosion measurements on steel with a similar chemical composition demonstrated an increased corrosion rate in a solution containing dissolved corrosion products compared to a reference solution. This accelerated corrosion was attributed to the acidity of akaganeite and iron (II) chloride, formed due to the vehicle's exposure to a humid and chloride-rich environment.

Keywords: car; corrosion; akaganeite; electrochemical methods; epoxy coatings.

INTRODUCTION

Corrosion poses a significant threat to the longevity and reliability of automobiles, impacting both their structural integrity and aesthetic appeal. From environmental factors like road salts and pollutants to inherent material vulnerabilities,

* Corresponding author. E-mail: bojana.radojkovic@ihtm.bg.ac.rs
https://doi.org/10.2298/JSC250327050P

vehicles are susceptible to various forms of corrosion that can compromise their performance.[1,2] Understanding the mechanisms and factors that contribute to automotive corrosion is crucial for developing effective prevention and mitigation strategies.[3–5] Numerous studies have examined corrosion failures in specific automotive components, providing valuable insights into real-world scenarios.[6–16]

Electrochemical corrosion, a primary cause of metal degradation, arises from chemical reactions between the metal surface and its environment.[17] This process involves anodic and cathodic reactions, leading to the dissolution of the metal in the presence of water or humidity. In the case of steel, a common material in automobiles, electrochemical corrosion results in the formation of iron oxy-hydroxides (FeO(OH)) on the surface.[18–20] These corrosion products, such as goethite (α-FeO(OH)) and lepidocrocite (γ-FeO(OH)), can sometimes form a protective layer, slowing down further corrosion. However, localized corrosion can still occur depending on the specific type of corrosion products present.

Akaganeite (β-FeO(OH)), another crystalline form of corrosion product, forms in humid environments with high chloride ion concentrations.[21–23] The incorporation of chloride ions into its crystal lattice makes akaganeite stable but also compromises its protective capabilities. The formation of akaganeite is facilitated at room or lower temperatures, under slightly acidic to neutral conditions (pH values from 4 to 7). If chloride ions are present to a lesser extent, then (instead of akaganeite) goethite, lepidocrocite and sometimes misawite (δ-FeO(OH))[18–20] are formed. Unlike goethite and lepidocrocite, akaganeite offers minimal protection against further corrosion. It is considered that the presence of akaganeite in steel corrosion products is a sign of its active corrosion.

This study investigates an instance of significant corrosion observed in the interior metal components of a relatively new automobile from a known brand, used by a rental car company in Serbia. Despite no visible signs of chemical spills or damage inside the vehicle, substantial corrosion was evident. The research aims to identify potential chemical residues on the carpet and upholstery and analyze the corrosion products on the steel surfaces. By employing instrumental methods such as Fourier-transform infrared spectroscopy (FTIR) and X-ray diffraction (XRD), the composition of the organic coating and corrosion products were determined.

Furthermore, the corrosion resistance of steel (AISI 4130), which is similar in composition to the steel used in the analyzed automobile, was directly compared in a solution containing dissolved corrosion products versus a standard solution. Electrochemical methods, including electrochemical impedance spectroscopy (EIS), linear polarization resistance (*LPR*), and the linear sweep voltammetry (LSV, Tafel method) were applied to study the corrosion properties of investigated specimens.

The investigation revealed that the corrosion of the automobile's interior steel components is likely the result of exposure to a humid environment rich in chlorides rather than improper use during its short operational period. The inadequately crosslinked epoxy coating was found to be permeable to moisture and chlorides, contributing to the corrosion process. Additionally, the presence of akaganeite and iron (II) chloride in the corrosion products, along with the moderately acidic nature of the solution, indicates ongoing corrosion activity that necessitates further attention to protective measures in automotive design.

EXPERIMENTAL

Materials

The AISI 4130 steel (25CrMo4 according to the EN standard) used in this study belongs to the category of low-alloy Cr-Mo steels. The purity and source of all employed materials were verified before experimentation. Table I lists the chemical composition of the tested steel AISI 4130, according to the standard,[24] and the actual chemical composition determined by the XRF method (Olympus Vanta C Series Handheld XRF Analyzer).

TABLE I. Chemical composition of tested steel, wt. %

Composition	C	Mn	P	S	Si	Cr	Mo
Standard	0.28–0.33	0.40–0.60	0.035	0.040	0.15–0.35	0.80–1.1	0.15–0.25
Measured	–	0.49	0.023	0.038	0.43	0.88	0.21

Corrosion product analysis

The composition of the corrosion products extracted from corroded steel parts within the automobile was analyzed using a Nicolet iS10 (Thermo Scientific) Fourier transform infrared (FTIR) spectrometer. FTIR spectra were recorded over a range of 4000-400 cm^{-1} with a resolution of 4 cm^{-1} at room temperature. Additionally, a Philips PW 1710 powder diffractometer (XRD) was employed to analyze the steel corrosion products under the following conditions: an operating voltage of 40 kV, a current strength of 30 mA, with copper (Cu) as the anticathode (wavelength CuKα, 1.54178 Å). The test range was set from 2θ 4 to 65°, with a step size of 2θ 0.01° and a recording rate of 5 ° min^{-1}.

Electrochemical measurements

A standard condensate solution served as the comparison solution for the electrochemical corrosion measurements. Corrosion products from the steel parts were added to this standard solution until saturation was achieved, followed by thorough mixing and three-stage squeezing to extract dissolved substances.

Corrosion measurements were conducted in both the standard solution prior to adding corrosion products and in the saturated solution containing dissolved corrosion products. The pH values of both solutions were determined using a pH meter (HI 2210 Hanna Instruments), with a precision of 0.01 pH unit.

The linear polarization resistance (*LPR*) method was utilized to determine the corrosion current density and the corrosion rate. The polarization resistance (R_p) is defined as the slope of the potential–current density curve ($\Delta E/\Delta j$) at the corrosion potential (E_{corr}). The relationship between R_p and the corrosion current density (j_{corr}) is given by:[25]

$$R_p = B/j_{corr} \quad (1)$$

where B is a constant that depends on the anodic (b_a) and the cathodic (b_c) Tafel slopes, calculated as:

$$B = b_a b_c / 2.3(b_a + b_c) \quad (2)$$

For low-alloy steels in neutral solutions containing chloride ions, B is typically set at 25 mV.[26] The conversion of j_{corr} into the corrosion rate (v_{corr} in mm year^{-1}) was performed using Faraday's law:

$$v_{corr}(\text{mm year}^{-1}) = 0.01166 j_{corr}(\mu\text{A cm}^{-2}) \quad (3)$$

while the values for the constant were obtained from ASTM G1 and ASTM G102.[27,28]

Electrochemical impedance spectroscopy (EIS) measurements involved applying a sinusoidal voltage of ±10 mV amplitude across a frequency range from 100000 to 0.001 Hz, with the system responses recorded as real and imaginary impedance components. The values of j_{corr} and v_{corr} were also obtained by Linear sweep voltammetry (LSV, Tafel method). After establishing a stable corrosion potential (E_{corr}), the working electrode was polarized from –0.25 to 0.25 V relative to E_{corr} at a sweep rate of 0.5 mV s^{-1}. In all electrochemical measurements, a saturated calomel electrode (SCE) served as the reference electrode, while a Pt-grid acted as the auxiliary electrode. All electrochemical methods were conducted using a Gamry 620 potentiostat/galvanostat device.

RESULTS AND DISCUSSION

Corrosion damage: visual evidence from the automobile interior

A detailed visual inspection of the automobile interior was carried out, and appropriate photographs were taken. The automobile interior looked new and preserved without any visible mechanical or other failure. Fig. 1a shows the exterior view of the automobile's back seat. There is no noticeable damage on the upholstered parts of the rear bench and the upholstery looks brand new. The carpet on the automobile floor also seems to be preserved, without damage. The carpet in the trunk was clean completely and undamaged as well (Fig. 1b). There are no traces of liquid spillage (water stains, aggressive liquids, etc.), nor visible external damage to the carpet in the trunk.

Fig. 1. Exterior view of: a) the back seat of the car and b) the carpet in the automobile trunk.

However, corrosion was observed on various metal components located in the double bottom of the automobile trunk. Specifically, the metal parts around the spare wheel exhibited corrosion, and the towing hook was completely corroded.

Significant corrosion was also evident on the automobile jack (Fig. 2a), with the surfaces of these components entirely coated in characteristic yellow––brown to brown corrosion products. Upon removing the seat upholstery, corrosion was found on the seat frame and axle, similarly covering their entire surfaces (Fig. 2b). Notably, the sponge and seat material showed no signs of water stains, chemical residue, or other liquids that might have contributed to the corrosion of these metal parts; they appeared undamaged and well-preserved.

Fig. 2. Corrosion of: a) the automobile jack components and b) the frame and shaft inside.

Beneath the dashboard, behind the control pedals, extensive corrosion of several metal components was evident (Fig. 3a). These parts were entirely covered with the characteristic yellow–brown to brown corrosion products. Lifting the protective cover on the rear seat revealed similarly complete corrosion on some metal components (Fig. 3b). Galvanized screws were used to fasten the protective covers. Zinc is expected to corrode preferentially, thereby protecting the steel from corrosion. However, the steel components exhibited extensive corrosion while the zinc coating on the screws remained intact.

Fig. 3. Corrosion of: a) the steel components under the control panel and b) the steel parts under the protective mask on the rear seat.

When steel objects lack adequate corrosion protection, they corrode much faster than galvanized screws. Thus, under the prevailing corrosive conditions, the

zinc coating effectively protected the screws, but it was insufficient to prevent corrosion of the surrounding steel parts.

Building upon the previously observed corrosion patterns, Fig. 4 further illustrates instances of corrosion failure on steel parts within the automobile's interior. The surfaces of these components are entirely covered in characteristic yellow-brown to brown steel corrosion products, consistent with previous findings. Notably, Fig. 4d reveals significant corrosion along the edges of a corroded steel part, along with layers of powdery steel corrosion products, suggesting that the corrosion process occurred over an extended period.

Fig. 4. Corrosion of steel parts.

To further investigate the nature of the corrosive environment, pH measurements were taken. The solution derived from a sample of corrosion products obtained from the corroded steel parts exhibited a pH of 3.45, indicating moderate acidity. In contrast, the standard solution used for comparison registered a pH of 5.70, confirming its near-neutral character. Furthermore, the solution resulting from washing a carpet sample taken from the automobile floor showed a neutral pH of 6.92. These pH values support the conclusion that the corrosion products themselves created a moderately acidic environment, while the carpet remained neutral. This neutrality suggests that the corrosion was unlikely caused by an acid

spillage onto the carpet, nor did any acid appear to have permeated through the carpet to induce steel corrosion.

Characterization of corrosion products and organic coatings via *FTIR spectroscopy*

FTIR analysis of the corrosion products (Fig. 5) revealed characteristic peaks at 3348 and 1614 cm^{-1}, corresponding to asymmetric and symmetric O–H stretching vibrations, respectively. Additionally, bands observed at 844 and 639 cm^{-1} can be attributed to –OH bending modes, indicative of the presence of β-FeOOH.[29–32] The presence of chloride ions in the corrosion products can be observed based on the base peak at the 420 cm^{-1} wavelength, which originates from an acid chlorides in-plane deformation.[33]

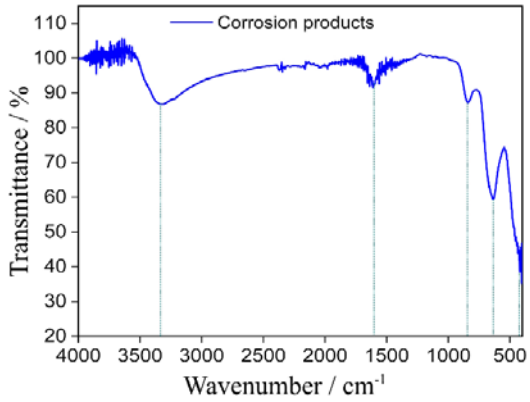

Fig. 5. FTIR diagram of steel corrosion products.

Given the extensive corrosion observed on the steel components, assessing the thickness and adhesion of the original organic coating proved challenging. On many components, the coating was absent, while on others, it was peeling away from the metal surface (Fig. 6). As a result, our analysis focused on determining the composition of the remaining coating fragments using FTIR spectroscopy.

Fig. 6. Appearance of the applied organic coating (paint) on the surface of the towing hook.

Fig. 7 shows the characteristic peaks obtained during the examination of the organic coating by the FTIR method. The organic coating contains a series of peaks corresponding to aromatic and aliphatic organic compounds, as well as an epoxy group, which is present in epoxy coatings.[34]

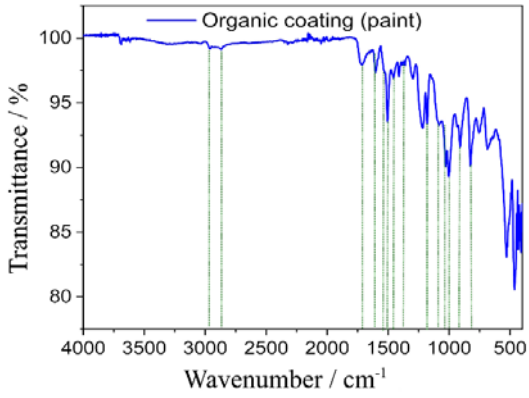

Fig. 7. Characteristic peaks obtained during the examination of the organic coating by the FTIR method.

The non-crosslinked epoxy coating (paint) has two characteristic peaks, which indicate the presence of the epoxy group: the first peak is located in the range of wavelengths from 3060 to 3000 cm^{-1}, while the second peak is located in the range of wavelengths from 960 to 810 cm^{-1} and it refers to the C–O deformation of the epoxy group.[35–39] The presence of peaks at 910 and 826 cm^{-1} wavelengths on the FTIR diagram (Fig. 7) indicates that the epoxy coating was not properly crosslinked. However, the absence of peaks in the range of wavelengths from 3060 to 3000 cm^{-1} is a sign that the epoxy coating is still partially crosslinked.[35–39]

In addition to the identification of peaks that are particularly characteristic of the epoxy group, other peaks that are also characteristic of the epoxy coating were identified. The peaks at 2965, 2863, 1456 and 1383 cm^{-1} wavelengths correspond to asymmetric and symmetric CH stretching of aromatic and aliphatic organic compounds.[37–40] The peak at wavelength 1602 cm^{-1} indicates the presence of the C=C group, and the peaks at the wavelengths 1531 and 1505 cm^{-1} indicate the presence of C–C stretching. The peak at 1180 cm^{-1} wavelengths corresponds to C–O stretching.[36] Also, the presence of the esters group (C=O) can be seen based on the peak at 1713 cm^{-1}, and the presence of the ethers group (C–O–C) is confirmed by peaks in the range of wavelengths from 1100 to 1000 cm^{-1}.[37]

The scheme structure of an epoxy resin before crosslinking is present in Fig. 8. It can be seen that the epoxy polymer on the ends of the molecule contains a characteristic epoxy group in the form of a three-angle. During curing, the characteristic epoxy group is opened, enabling proper epoxy coating cross-linking.

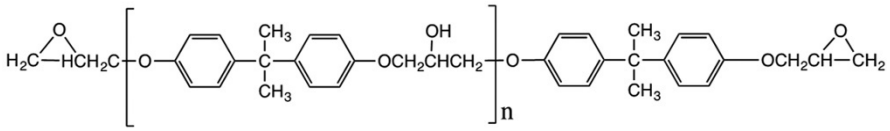

Fig. 8. Scheme structure of the epoxy polymer before crosslinking.

The inadequate cross-linking of the epoxy coating can be attributed to an improper curing process, such as curing at insufficiently high temperatures and/or for an inadequate duration. This incomplete crosslinking results in a porous coating, allowing chloride ions and moisture to penetrate through the pores, thereby creating favorable conditions for corrosion to occur. Additionally, the poorly crosslinked epoxy coating is brittle, making it prone to peeling from the steel surface. The weak adhesion of the coating may also stem from inadequate surface preparation or cleaning of the steel components before the application of the coating. These factors collectively explain the observed condition of the organic coating in the automobile and its inability to provide effective corrosion protection.

XRD characterization of corrosion products

The XRD analysis of the corrosion products collected from the automobile (Fig. 9) identified two crystalline phases: *β*-FeO(OH) (ferric oxy-hydroxide) and $FeCl_2 \cdot 4H_2O$. Semi-quantitative analysis showed that *β*-FeO(OH) accounted for approximately 88 wt. % of the corrosion products, while $FeCl_2 \cdot 4H_2O$ made up about 12 wt. %. The *β*-FeO(OH), also known as akaganeite, crystallizes in a monoclinic structure within space group I2/m (No. 12). Literature indicates that akaganeite requires chloride ions to stabilize its structure, with its formula more accurately represented as $FeO_{0.833}(OH)_{1.167}Cl_{0.167}$.[41] In its structure, octahedral chains form tunnels that are partially filled with chloride ions, occupying approximately two-thirds of the available sites. Hydrogen bonds between chlorides and surrounding hydrogen further stabilize the structure. At temperatures above 200 °C, akaganeite releases chloride ions and transforms into hematite Fe_2O_3, a more stable phase. The crystal structure and microstructure of akaganeite have been extensively documented in the literature.[21,22,42]

The identified phases are characteristic of steel corrosion under humid conditions with significant chloride ion presence. Akaganeite is commonly associated with active corrosion processes, while iron (II) chloride hydrate plays a role in sustaining these processes. In environments with lower chloride concentrations, alternative corrosion products such as goethite, lepidocrocite or misawite are typically formed, which tend to slow down steel corrosion compared to akaganeite. Thus, the presence of akaganeite in the analyzed sample indicates ongoing active

corrosion and suggests that the corrosive processes have persisted for a considerable period.

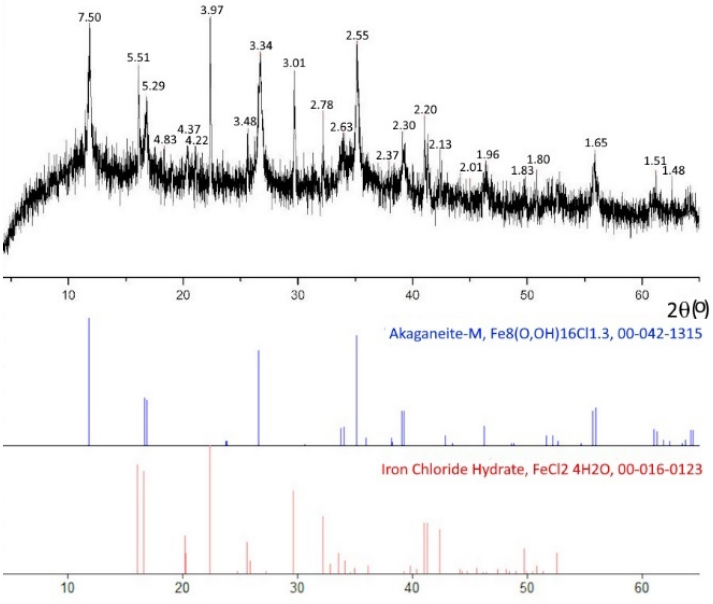

Fig 9. Diffractogram of the examined sample of corrosion products.

Iron (II) chloride present in the corrosion products undergoes hydrolysis in the presence of oxygen and moisture from the air, forming akaganeite, hydrogen ions, and additional chloride ions according to:[42]

$$2Fe^{2+} + 4Cl^- + 3H_2O + 1/2O_2 \rightarrow 2FeO(OH) + 4H^+ + 4Cl^- \quad (4)$$

The generated hydrogen and chloride ions further accelerate steel corrosion through the reaction described as:

$$2Fe + 4H^+ + 4Cl^- + O_2 \rightarrow 2Fe^{2+} + 4Cl^- + 2H_2O \quad (5)$$

The resulting Fe^{2+} and Cl^- re-enter the hydrolysis cycle described in Eq. (4), perpetuating a self-sustaining process known as the Askey cycle.[43] This cycle produces an acidic environment due to H^+ generation and continuously forms akaganeite (β-FeO(OH)). The presence of akaganeite is thus a clear indicator of active steel corrosion.

As previously noted, no evidence of an acidic liquid spillage was observed on the carpet covering the corroded steel parts. The solution obtained by washing carpet particles exhibited a neutral pH while the solution containing dissolved corrosion products was acidic. This confirms that the corrosion was not caused by

external acidic substances penetrating through the carpet but rather by environmental factors such as moisture, oxygen, and chloride ions.

The non-properly crosslinked epoxy coating on the steel surface further facilitated corrosion. Its porous and brittle nature allowed moisture and chloride ions to diffuse through to the steel surface, initiating and sustaining the Askey cycle.[43] This continuous regeneration of hydrogen and chloride ions promotes an acidic environment conducive to active corrosion. Only complete drying of the corrosion products, including akaganeite and iron (II) chloride hydrate, can disrupt this cycle and stop further degradation.

Electrochemical measurements

Linear polarization resistance (*LPR*) measurements were conducted to assess the corrosion resistance of steel in different solutions, and the results are presented in Fig. 10. As can be seen from Fig. 10, the polarization resistance (R_p) for steel in the solution containing corrosion products was 2.38 kΩ cm^2, while the R_p for steel in the standard solution was 3.28 kΩ cm^2.

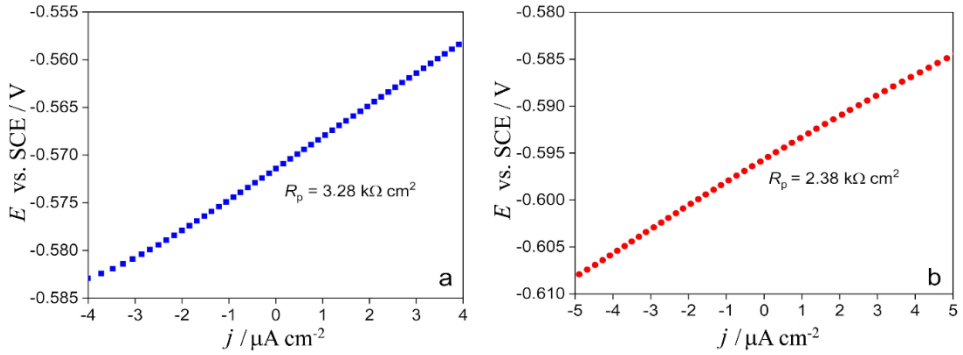

Fig. 10. Results of the *LPR* testing in: a) standard solution and b) solution obtained by dissolving corrosion products in the standard solution.

Therefore, *LPR* measurements indicated that the standard solution exhibited a higher R_p than the solution with dissolved steel corrosion products. This suggests that the corrosion products, which contain akaganeite (β-FeO(OH)) and iron (II) chloride, release hydrogen ions according to Reaction (4), creating a moderately acidic environment. It is well-established that the corrosion rate of steel is higher in acidic environments compared to neutral ones, which explains the lower R_p value observed in the solution containing corrosion products.

The main corrosion parameters obtained by the *LPR* method are presented in Table II.

The results of the electrochemical impedance spectroscopy (EIS) testing of steel are presented in Fig. 11. The equivalent electrical circuit (EEC) used to fit the

EIS data is shown in Fig. 11d. In this circuit, R_e represents the electrolyte resistance, R_p denotes the polarization resistance and CPE is the constant phase element that accounts for surface inhomogeneities of the tested steel.

TABLE II. Test results using the *LPR* method

Solution	R_p / kΩ cm^2	j_{corr} / μA cm^{-2}	v_{corr} / mm year^{-1}
Standard	3.28	7.62	0.089
Standard + corrosion product	2.38	10.5	1.22

The polarization resistance values obtained from the EIS measurements, based on both the Nyquist and Bode modulus diagrams (Fig. 11), revealed that the R_p value for steel in the solution containing dissolved corrosion products was 1.67 kΩ cm^2, while in the standard solution it was higher, at 2.64 kΩ cm^2.

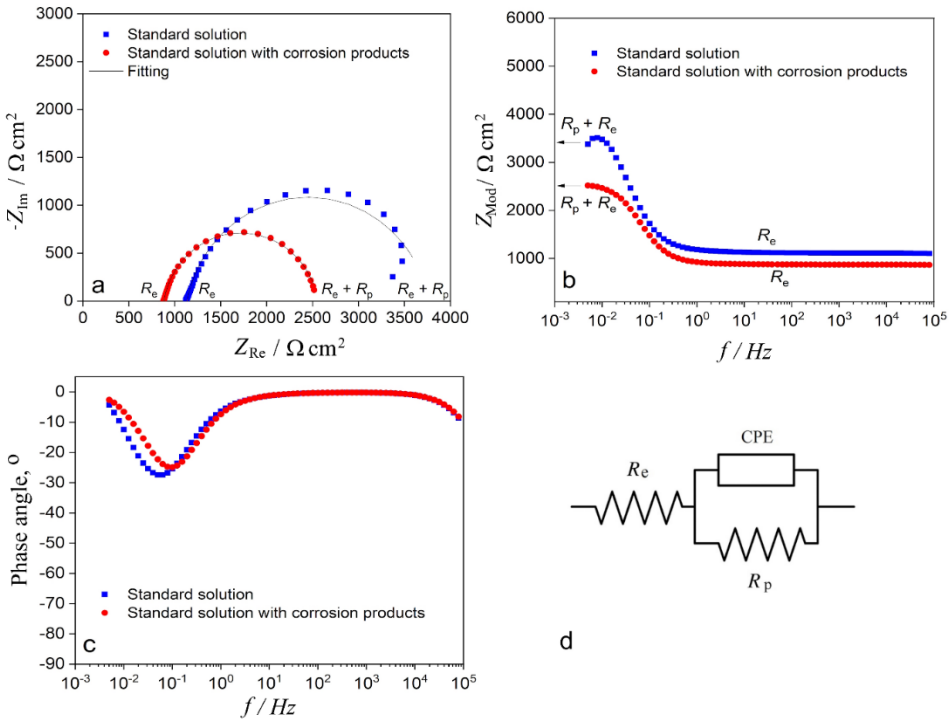

Fig 11. Results of the EIS test in the standard solution and in the standard solution in which corrosion products are dissolved; a) Nyquist diagrams, c) Bode modulus diagrams, c) Bode phase diagrams and d) equivalent electric circuit (EEC).

The polarization resistance (R_p) values obtained by the EIS method are consistent with the results obtained from the *LPR* method. Specifically, a lower R_p value was recorded for the solution containing dissolved corrosion products com-

pared to the pure standard solution, which is also reflected in Tables II and III. This reduction in polarization resistance is attributed to the moderate acidity present in the solution with dissolved corrosion products.

TABLE III. The results of the EIS method

Solution	R_e	R_p	CPE		C_{eff}	j_{corr}	v_{corr}
	kΩ cm^2	kΩ cm^2	Q / mΩ^{-1} s^n cm^{-2}	n	mF cm^2	μA cm^{-2}	mm year^{-1}
Standard	1.13	2.64	1.545	0.875	1.889	9.47	0.110
Standard + corrosion product	0.88	1.67	1.578	0.899	1.759	15.0	0.175

Additionally, Table III presents the effective capacitance (C_{eff}), calculated using the Brug Equation,[44] which incorporates values for R_p, Q and n from the same table:

$$C_{eff} = R_p^{(1-n)/n} Q^{1/n} \quad (6)$$

The C_{eff} value for specimens tested in the standard solution is somewhat higher than that for specimens exposed to the solution containing corrosion products.

Furthermore, Fig. 11 indicates a relatively high electrolyte resistance (R_e), attributed to the low concentration of ions in the tested solutions. In contrast, the electrolyte resistance is lower in the solution with dissolved steel corrosion products due to the presence of hydrogen ions.

The Bode phase diagram further supports these observations, revealing that steel exhibits reduced corrosion resistance in the standard solution containing corrosion products (Fig. 11 c and Table III) compared to the pure standard solution. The narrowing of the peak at low frequencies reinforces this conclusion, along with a shift of the peak towards higher frequencies, consistent with the literature findings.[45]

Linear sweep voltammetry (LSV) testing of steel (Fig. 12) revealed a higher corrosion current density (j_{corr}) in the solution containing dissolved corrosion products compared to the standard solution. Specifically, the j_{corr} value for steel in the solution with corrosion products was 11 μA cm^{-2}, while in the standard solution, it was 5 μA cm^{-2}. The corrosion rate values (v_{corr}) were then calculated using Faraday's law based on the measured j_{corr} values (Table IV).

These results demonstrate that the presence of corrosion products increases the corrosion rate, which is consistent with the findings from the *LPR* and EIS measurements. This increased corrosion rate is attributed to the acidic environment generated by akaganeite (β-FeO(OH)) and iron (II) chloride present in the corrosion products, according to Reaction (4).

While the absolute corrosion rate values vary somewhat depending on the method used (*LPR*, EIS or LSV), all methods consistently indicated a higher steel

corrosion rate in the solution containing dissolved corrosion products compared to the standard solution.

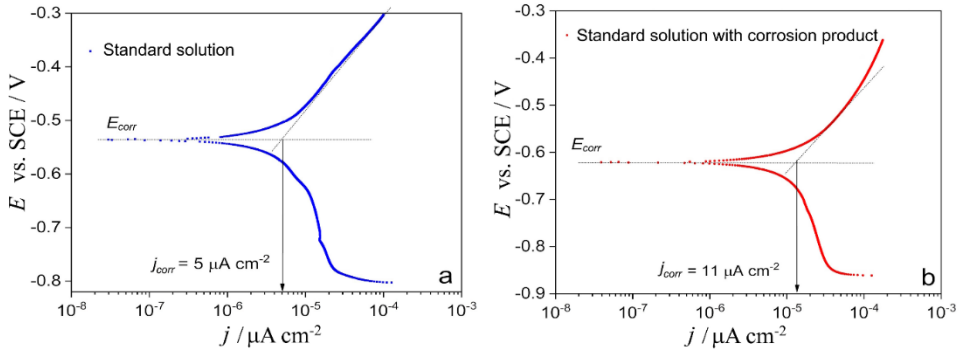

Fig. 12. Results of testing steel by the Tafel method in: a) the standard solution and b) the solution obtained by dissolving corrosion products in the standard solution.

TABLE IV. The results of the LSV test

Solution	j_{corr} / μA cm^{-2}	v_{corr} / mm year^{-1}
Standard	5	0.058
Standard + corrosion products	11	0.128

CONCLUSION

In conclusion, the evidence suggests that the observed corrosion within the automobile was likely initiated before its short-term use. Visual inspection ruled out a spillage as a cause, while XRD and FTIR analyses identified akageneite (β-FeO(OH)) and iron (II) chloride within the corrosion products, indicating a chloride-rich environment. The presence of akaganeite, a known indicator of active corrosion, suggests that the steel components were exposed to humidity and chlorides, possibly during storage. Furthermore, the epoxy coating's improper crosslinking, as revealed by FTIR, would have compromised its protective capabilities, allowing corrosive agents to reach the metal surface. Electrochemical measurements confirmed these findings, demonstrating a higher corrosion rate in solutions containing the identified corrosion products. This study highlights the importance of proper material selection, storage conditions, and coating application techniques in preventing premature corrosion in automotive components, ultimately extending the lifespan and reliability of vehicles.

Preprint note. This article has its preprint version on the preprint server, available on http://dx.doi.org/10.2139/ssrn.4981934

Acknowledgement. This work was supported by the Ministry of Science, Technological Development and Innovation of the Republic of Serbia (Grant No. 451-03-66/2024-03/ /200026, 451-03-66/2024-03/ 200175 and 451-03-65/2024-03/ 200135).

ИЗВОД

ИСПИТИВАЊЕ УЗРОКА КОРОЗИЈЕ И ОШТЕЋЕЊА УНУТРАШЊИХ МЕТАЛНИХ КОМПОНЕНАТА АУТОМОБИЛА

ЈОВАНКА Н. ПЕЈИЋ[1], БОРЕ В: ЈЕГДИЋ[1], БОЈАНА М. РАДОЈКОВИЋ[1], АНЂЕЛА Р. СИМОВИЋ[1], ДУЊА Д. МАРУНКИЋ[1], БРАНИМИР З. ЈУГОВИЋ[2] и АЛЕКСАНДРА С. ПОПОВИЋ[3]

[1]Универзитет у Београду, Институт за хемију, технологију и металургију, Његошева 12, Београд, [2]Институт техничких наука Српске академије наука и уметности, Кнез Михаилова 35, Београд и [3]Универзитет у Београду, Технолошко–металуршки факултет, Карнегијева 4, Београд

У раду су испитане размере корозије и основни узроци оштећења унутрашњих металних компоненти аутомобила познате марке, који је у власништву компаније за изнајмљивање аутомобила у Србији и који је био у употреби годину дана. Унутрашњост аутомобила, тапациринзи и тепих на поду аутомобила, су очувани, без трагова оштећења, а такође није утврђено присуство неке корозивне хемикалије. Раствор настао после испирања делова тепиха узетог са пода аутомобила се понашао неутрално. Корозивно понашање анализираних узорака одређено је коришћењем спектроскопије електрохемијске импеданције, линеарне поларизационе отпорности и линеарне волтаметрије. Резултати анализе методама рендгенске дифракције (XRD) и инфрацрвене спектроскопије са Фуријеовом трансформацијом (FTIR) показали су да производи корозије узети са кородираних челичних делова садрже акаганеит (β-FeO(OH)) и гвожђе(II)-хлорид. FTIR анализа органске превлаке открила је да је примењена епоксидна превлака недовољно умрежена, што је чини пропусном за влагу и хлоридне јоне. Електрохемијска мерења корозије на челику сличног хемијског састава са челиком коришћеним за израду аутомобила су показала повећану брзину корозије у раствору који садржи растворене производе корозије у поређењу са референтним раствором. Ова убрзана корозија приписује се киселости акаганеита и гвожђе(II)-хлорида, који су настали услед изложености делова возила влажном и хлоридима богатом окружењу.

(Примљено 27. марта, ревидирано 17. априла, прихваћено 10. јула 2025)

REFERENCES

1. L. J. Korb, D. L. Olson, in *ASM Handbook, Volume 13: Corrosion*, ASM International, Materials Park, OH, 1987
2. A. Kumar, J. Singh, *Proc. Eng. Sci.* **4** (2022) 13 (https://doi.org/10.24874/PES04.01.003)
3. D. Mizuno, S. Suzuki, S. Fujita, N. Hara, *Corros. Sci.* **83** (2014) 217 (http://dx.doi.org/10.1016/j.corsci.2014.02.020)
4. K. Dhonde, M. Mirhassani, E. Tam, S.Sawyer-Beaulieu, *Materials* **15** (2022) 3211 (https://doi.org/10.3390/ma15093211)
5. S. Sawyer-Beaulieu, E. Tam, A. Hussein, *Materials* **15** (2022) 3053 (https://doi.org/10.3390/ma15093053)
6. E. Díaza, L. Soria, J. M. Gallardo, *Eng. Fail. Anal.* **105** (2019) 828 (https://doi.org/10.1016/j.engfailanal.2019.07.022)
7. F. Bergh, G.C. Silva, C. Silva, P. Paiva, *Eng. Fail. Anal.* **129** (2021) 105679 (https://doi.org/10.1016/j.engfailanal.2021.105679)
8. J. Gweon, J. Park, W.K. Lee, D.Y. Kim, H. Jang, *Eng. Fail. Anal.* **128** (2021) 105583 (https://doi.org/10.1016/j.engfailanal.2021.105583)
9. C. Langer, W. Wendland, K. Honold, L. Schmidt, J.S. Gutmann, M. Dornbusch, *Eng. Fail. Anal.* **91** (2018) 255 (https://doi.org/10.1016/j.engfailanal.2018.04.031)

10. D. H. Sohn, Y. Lee, H. J. Jang, S. Y. Cho, *Corros. Sci. Technol.* **21** (2022) 1 (https://doi.org/10.14773/cst.2022.21.1.1)
11. L. Kosec, A. Nagode, G. Kosec, D. Kovacevic, B. Karpe, B. Zorc, B. Kosec, *Case Stud. Eng. Fail. Anal.* **4** (2015) 100 (http://dx.doi.org/10.1016/j.csefa.2013.12.004)
12. N. Solomon, I. Solomon*, Eng. Fail. Anal.* **92** (2018) 44 (https://doi.org/10.1016/j.engfailanal.2018.04.049)
13. M. Torkar, M. Godec, *Eng. Fail. Anal.* **10** (2003) 325 (https://doi.org/10.1016/S1350-6307(02)00069-9)
14. M. Godec, Dj. Mandrino, M. Jenko*, Eng. Fail. Anal.* **16** (2009) 1252 (https://doi.org/10.1016/j.engfailanal.2008.08.022)
15. M. I. Khana, M. A. Khan, A. Shakoor, *Eng. Fail. Anal.* **85** (2018) 77 (https://doi.org/10.1016/j.engfailanal.2017.12.001)
16. E. Arslan, K. Genel, *Eng. Fail. Anal.* **153** (2023) 107569 (https://doi.org/10.1016/j.engfailanal.2023.107569)
17. R. W. Revie, H. H. Uhlig, *Corrosion and Corrosion Control: An Introduction to Corrosion Science and Engineering*, John Wiley and Sons, Hoboken, NJ, 2008 (https://doi.org/10.1002/9780470277270)
18. J. Labbe, J. Ledion, F. Hui, *Corros. Sci.* **50** (2008) 1228 (https://doi.org/10.1016/j.corsci.2007.08.023)
19. T. Misawa, T. Kyuno, W. Suetaka, S. Shimodaira, *Corros. Sci.* **11** (1971) 35 (https://doi.org/10.1016/S0010-938X(71)80072-0)
20. T. Misawa, T. Kyuno, W. Suetaka, S. Shimodaira, *Corros. Sci.* **14** (1974) 279 (https://doi.org/10.1016/S0010-938X(74)80037-5)
21. S. Reguer, F. Mirambet, E. Dooryhee, J. Hodeau, P. Dillmann, P. Lagarde, *Corros. Sci.* **51** (2009) 2795 (https://doi.org/10.1016/j.corsci.2009.07.012)
22. K. Stahl, K. Nielsen, J. Jiang, B. Lebech, J. Hanson, P. Norby, J. Lanschot, *Corros. Sci.* **45** (2003) 2563 (https://doi.org/10.1016/S0010-938X(03)00078-7)
23. M. Gilberg, N. Seeley, *Stud. Conserv.* **26** (1981) 50 (https://doi.org/10.1179/sic.1981.26.2.50)
24. *ASTM A29: Standard Specification for General Requirements for Steel Bars, Carbon and Alloy, Hot-Wrought*, ASTM International, West Conshohocken, PA, 2023
25. *ASTM-G59: Standard Test Method for Conducting Potentiodynamic Polarization Resistance Measurements*, ASTM International, West Conshohocken, PA, 2023
26. S. Papavinasamt, in *Techniques for corrosion monitoring*, L. Yang, Ed., Woodhead Publishing, Cambridge, 2008, p. 49 (https://doi.org/10.1016/B978-0-08-103003-5.00003-5)
27. *ASTM G1: Standard Practice for Preparing, Cleaning, and Evaluating Corrosion Test Specimens*, ASTM International, West Conshohocken, PA, 2023
28. *ASTM G102: Calculation of Corrosion Rates and Related Information from Electrochemical Measurements*, ASTM International, West Conshohocken, PA, 2023
29. G. Nauer, P. Strecha, N. Brinda-Konopik, G. Liptay, *J. Therm. Anal.* **30** (1985) 813 (https://doi.org/10.1007/bf01913309)
30. S. Bashir, R. W. McCabe, C. Boxall, M. S. Leaver, D. Mobbs, *J. Nanopart. Res.* **11 (**2008) 701 (https://doi.org/10.1007/s11051-008-9467-z)
31. L. Mei, L. Liao, Z. Wang, C. Xu, *Adv. Mater. Sci. Eng.* **2015** (2015) 250836 (https://doi.org/10.1155/2015/250836)

32. M. Amini, Y. Mousazade, Z. Zand, M. Bagherzadeh, M. M. Najafpour, *Sci. Rep.* **11** (2021) 6642 (https://doi.org/10.1038/s41598-021-85672-x)
33. J. B. Lambert, H. F. Shurvell, R. G. Cooks, *Introduction to Organic Spectroscopy*, 1st ed., Macmillan, New York, 1987
34. P. Maity, S. V. Kasisomayajula, V. Parameswaran1, S. Basu, N. Gupta, *IEEE T. Dielect. El. In.* **15** (2008) 63 (https://doi.org/10.1109/T-DEI.2008.4446737)
35. S. Zlatković, G. S. Nikolić, J. V. Stamenković, *Chem. Ind.* **57** (2003) 563 (https://doi.org/10.2298/HEMIND0311563Z)
36. G. Nikolic, S. Zlatkovic, M. Cakic, S. Cakic, C. Lacnjevac, Z. Rajic, *Sensors* **10** (2010) 684 (https://doi.org/10.3390/s100100684)
37. M. G. González, J. C. Cabanelas, J. Baselga, in *Infrared Spectroscopy – Materials Science, Engineering and Technology*, T. Theophanides Ed., InTech, London, 2012 (https://doi.org/10.5772/36323)
38. L.A. Teixeira, V.D.L. Junior, S.M. da Luz, in *Proceedings of 16th Brazilian Polymer Conference (16 CBPOL)*, Ouro Preto-MG, Brazil, October 24–28, 2021, p. 1338 (http://e-democracia.com.br/cbpol/anais/2021/pdfs/plenary/4DPJ.pdf)
39. D. S. Achilias, M. M. Karabela, E. A. Varkopoulou, I. D. Sideridou*, J. Macromol. Sci., A* **49** (2012) 630 (https://doi.org/10.1080/10601325.2012.696995)
40. N. Rajagopalan, A. S. Khanna, *J. Coat.* **2014** (2014) 515470 (https://doi.org/10.1155/2014/515470)
41. C. Rémazeilles, Ph. Refait, *Corros. Sci.* **49** (2007) 844 (https://doi.org/10.1016/j.corsci.2006.06.003)
42. L. S. Selwyn, in *ASM Handbook, Volume 13C: Corrosion: Environments and Industries*, S. D. Cramer, B. S. Covino, Jr., Eds., ASM International, Materials Park, OH, 2006, p. 306 (ISBN**:** 978-0-87170-709-3)
43. A. Askey, S. B. Lyon, G. E. Thompson, J. B. Johnson, G. C. Wood, M. Cooke, P. Sage, *Corros. Sci.* **34** (1993) 233 (https://doi.org/10.1016/0010-938X(93)90004-Z)
44. B. Hirschorn, M. E. Orazem, B. Tribollet, V. Vivier, I. Frateur, M. Musiani, *J. Electrochem. Soc.* **157** (2010) C458 (https://doi.org/10.1149/1.3499565)
45. L. G. Ecco, S. Rossi, F. Deflorian, M. Fedel, *J. Electrochem. Soc.* **165** (2018) C933 (https://doi.org/10.1149/2.0371814jes).